

## Spontaneous formation of polar superfluid droplets in a $p$ -wave interacting Bose gas

Zehan Li <sup>1</sup>, Jian-Song Pan <sup>2,\*</sup> and W. Vincent Liu <sup>1,2,3,†</sup>

<sup>1</sup>*Department of Physics and Astronomy, University of Pittsburgh, Pittsburgh, Pennsylvania 15260, USA*

<sup>2</sup>*Wilczek Quantum Center, School of Physics and Astronomy and T. D. Lee Institute, Shanghai Jiao Tong University, Shanghai 200240, China*

<sup>3</sup>*Shenzhen Institute for Quantum Science and Engineering and Department of Physics, Southern University of Science and Technology, Shenzhen 518055, China*



(Received 23 July 2019; revised manuscript received 10 October 2019; published 21 November 2019)

We study the quantum fluctuations in the condensates of a mixture of bosonic atoms and molecules with interspecies  $p$ -wave interaction. Our analysis shows that the quantum phase of coexisting atomic and molecular condensates is unstable at the mean-field level. Unlike the mixture of  $s$ -wave interaction, the Lee-Huang-Yang correction of  $p$ -wave interaction is unexpectedly found here to exhibit an opposite sign with respect to its mean-field term above a critical particle density. This quantum correction to the mean-field energy provides a remarkable mechanism to self-stabilize the phase. The order parameter of this superfluid phase carries opposite finite momenta for the two atomic species while the molecular component is a polar condensate. Such a correlated order spontaneously breaks a rich set of global U(1) gauge, atomic spin, spatial rotation and translation, and time-reversal symmetries. For potential experimental observation, the phenomenon of anisotropic polar superfluid droplets is predicted to occur when the particle number is kept finite.

DOI: [10.1103/PhysRevA.100.053620](https://doi.org/10.1103/PhysRevA.100.053620)

### I. INTRODUCTION

Quantum fluctuation is one of the most intrinsic properties of quantum mechanics, which is responsible for many fascinating physical phenomena, such as Casimir effect and abundant quantum phase transitions. Recently, Petrov showed that quantum fluctuation reflected by Lee-Huang-Yang (LHY) correction can prevent a mean-field-unstable Bose gas from collapsing [1]. The competition between the mean-field attraction and LHY repulsion stabilizes the Bose gas into a self-bound liquidlike droplet state. Subsequently, several experimental groups reported this novel quantum state with the prediction of Petrov [2–4]. In order to protrude the action of LHY correction, which is typically small in the dilute limit, Petrov suggested to subtly balance the inter- and intraspecies interactions at the mean-field level. Owing to its unique formation mechanism, the self-bound state shows many interesting features, such as the quantum droplet is self-trapped and evaporated without external potential [1,5].

The properties of the quantum droplet are linked to the properties of interaction between particles. It is natural to ask if quantum droplets can be stabilized with other types of interaction and what their properties might be. It was also found that quantum droplets can be stabilized in a dipolar Bose gas, benefiting from the competition between the dipolar interaction and  $s$ -wave contact interaction [6–9]. The quantum droplets in a dipolar Bose gas are anisotropic and form a regular array as a consequence of the dipolar interaction being anisotropic and long ranged. Moreover, it is also predicted

quantum droplets can be stabilized with the assistance of three-body interaction [10,11] and spin-orbit coupling [12].

Here we study the beyond-mean-field ground state of a  $p$ -wave interacting Bose gas, and predict the existence of a finite-momentum anisotropic self-stabilized quantum droplet. At the mean-field level, this  $p$ -wave interacting Bose gas typically has three ground-state phases: an atomic superfluid phase with only the atomic condensate, an atomic-molecular superfluid phase with both atomic and molecular condensates, and a molecular superfluid phase with only the molecular condensate. We find the AMSF phase is unstable and tends to collapse. Unlike pure  $s$ -wave interaction [13], we find the sign of the LHY correction of  $p$ -wave interaction may be different from that of the mean-field term when varying particle densities. A balance between the mean-field part and LHY correction exists for certain particle densities, which gives rise to a self-stabilized (-bound) state without external potential. It is shown that the self-stabilized state even survives in the dilute limit estimated with scattering volume. In addition to the U(1) global phase symmetry, the rotation, translation, and time-reversal symmetries are found to be spontaneously broken by the presence of a finite momentum of the order parameters. The resulting ground state is predicted to be an anisotropic quantum droplet with finite momentum for a system with finite particle number.

### II. MODEL

Inspired by the experimental observations of  $p$ -wave Feshbach resonance in the mixture of  $^{85}\text{Rb}$  and  $^{87}\text{Rb}$  atoms [14,15], we consider a mixture of two distinguishable species of bosonic atoms respectively created by  $\hat{\psi}_1^\dagger(\mathbf{r})$  and  $\hat{\psi}_2^\dagger(\mathbf{r})$  with interspecies  $p$ -wave interaction. The  $p$ -wave interaction arises from a  $p$ -wave Feshbach resonance by coupling with

\*panjsong@sjtu.edu.cn

†wvliu@pitt.edu

TABLE I. Symmetry transformation.  $U_N(1)$ :  $\theta \in [0, 2\pi)$  is an arbitrary angle. This symmetry corresponds to the total number conservation.  $[SU(2)/U_y(1)]$  with spin-rotation symmetry  $U_y(1)$  generated by  $\sigma_y$ :  $\theta_x$  and  $\theta_z$  are arbitrary angles. Here  $\sigma_{x,y,z}$  are the Pauli matrices.  $SO(3)$ :  $\lambda_{x,y,z}$  are defined in Eq. (2), and  $\bar{\theta}_{x,y,z}$  are arbitrary rotation angles.  $\text{Tr}$  is the translation symmetry:  $\mathbf{r}'$  is an arbitrary displacement vector in a 3D spatial coordinate.  $\mathcal{T}$  is time reversal, and we use momentum representation to expand the  $\hat{\psi}_1$  and  $\hat{\psi}_2$  fields. Due to momentum conservation, the momentum of the molecule fields is restricted to  $\mathbf{p}_1 + \mathbf{p}_2$ .

Symmetry	$\hat{\psi}_1(\mathbf{r})$	$\hat{\psi}_2(\mathbf{r})$	$\hat{\phi}_{x,y,z}(\mathbf{r})$	$\nabla$
$U_N(1)$	$e^{i\theta} \hat{\psi}_1$	$e^{i\theta} \hat{\psi}_2$	$e^{2i\theta} \hat{\phi}_{x,y,z}$	—
$[SU(2)/U_y(1)]$	$e^{i\theta_x \sigma_x + i\theta_z \sigma_z} (\hat{\psi}_1, \hat{\psi}_2)^T$		—	—
$SO(3)$	—	—	$e^{i \sum_{i=x,y,z} \bar{\theta}_i \lambda_i} \hat{\phi}$	$e^{i \sum_{i=x,y,z} \bar{\theta}_i \lambda_i} \nabla$
$\text{Tr}$	$\hat{\psi}_1(\mathbf{r} + \mathbf{r}')$	$\hat{\psi}_2(\mathbf{r} + \mathbf{r}')$	$\hat{\phi}_{x,y,z}(\mathbf{r} + \mathbf{r}')$	—
$\mathcal{T}$	$\sum_{\mathbf{p}_1} e^{-i\mathbf{p}_1 \cdot \mathbf{r}} \hat{a}_{1,-\mathbf{p}_1}$	$\sum_{\mathbf{p}_2} e^{-i\mathbf{p}_2 \cdot \mathbf{r}} \hat{a}_{2,-\mathbf{p}_2}$	$e^{-i(\mathbf{p}_1 + \mathbf{p}_2) \cdot \mathbf{r}} \hat{b}_{i,-\mathbf{p}_1 - \mathbf{p}_2}$	—

three closed molecular channels denoted by  $l_z = -1, 0, 1$ . Here  $l_z \hbar$  are the magnetic angular momentum carried by the molecules on the closed channels, which are created by  $\hat{\phi}_{l_z=-1,0,1}^\dagger(\mathbf{r})$ , respectively. It will be convenient to discuss the physics with bases  $\hat{\phi}_{i=x,y,z}^\dagger$ , which are related with  $\hat{\phi}_{l_z=-1,0,1}^\dagger$  through  $\hat{\phi}_{\pm 1}^\dagger = (\hat{\phi}_x^\dagger \pm i\hat{\phi}_y^\dagger)/\sqrt{2}$ , and  $\hat{\phi}_0^\dagger = \hat{\phi}_z^\dagger$ . To focus on the physics arising from  $p$ -wave interaction, we will restrict our attention to the case where the closed channels are degenerate and background (nonresonant) interactions are negligible. The system we consider is characterized by the Hamiltonian density

$$\mathcal{H} = \sum_{\sigma=1,2} \hat{\psi}_\sigma^\dagger \left( -\frac{\nabla^2}{2m} \right) \hat{\psi}_\sigma + \sum_{i=x,y,z} \hat{\phi}_i^\dagger \left( -\frac{\nabla^2}{4m} - \epsilon_0 \right) \hat{\phi}_i + \sum_{i=x,y,z} \left[ \frac{\bar{g}}{2} \hat{\phi}_i^\dagger (\hat{\psi}_1, \hat{\psi}_2) \sigma_y \partial_i (\hat{\psi}_1, \hat{\psi}_2)^T + \text{H.c.} \right], \quad (1)$$

where the atomic masses have been assumed to be the same, i.e.,  $m_1 = m_2 = m$ ,  $\epsilon_0$  is the detuning of molecule channels,  $\bar{g}$  represents the strength of  $p$ -wave interaction, and  $\sigma_y$  is the Pauli matrix. Here the reduced Plank constant  $\hbar$  has been set as 1.

Our model possesses  $U_N(1) \times [SU(2)/U_y(1)] \times SO(3) \times \text{Tr} \times \mathcal{T}$  symmetries, where  $U_N(1)$  is the global gauge symmetry,  $[SU(2)/U_y(1)]$  the spin-rotation symmetry around the  $x$  and  $z$  directions,  $SO(3)$  the three-dimensional spatial rotation symmetry,  $\text{Tr}$  the translation symmetry in the absence of an external field, and  $\mathcal{T}$  the time-reversal symmetry. The symmetry transformations are listed in Table I. It is worth noting that spin-rotation symmetry  $[SU(2)/U_y(1)]$  is reduced to a spin-rotation symmetry  $U_z(1)$  generated by  $\sigma_z$  in the presence of intraspecies  $s$ -wave interaction [16,17]. In  $SO(3)$  rotation symmetry, the atom fields are scalar fields, so they remain constant under  $SO(3)$  transformation. However, molecular field  $\hat{\phi}$  and gradient operator  $\nabla$  are all vector fields, and they are transformed by a 3D spatial rotation. In Table I, the generators of rotation symmetry  $\lambda_{x,y,z}$  are given by

$$\lambda_x = \begin{pmatrix} 0 & 0 & 0 \\ 0 & 0 & -i \\ 0 & i & 0 \end{pmatrix}, \lambda_y = \begin{pmatrix} 0 & 0 & i \\ 0 & 0 & 0 \\ -i & 0 & 0 \end{pmatrix}, \quad (2)$$

$$\lambda_z = \begin{pmatrix} 0 & -i & 0 \\ i & 0 & 0 \\ 0 & 0 & 0 \end{pmatrix}.$$

Time-reversal symmetry  $\mathcal{T}$  is given by reversing the momentum of atomic and molecular field operators, i.e., transforming  $\hat{a}_{1,\mathbf{p}_1}$ ,  $\hat{a}_{2,\mathbf{p}_2}$ , and  $\hat{b}_{i,\mathbf{p}_1+\mathbf{p}_2}$  as  $\hat{a}_{1,-\mathbf{p}_1}$ ,  $\hat{a}_{2,-\mathbf{p}_2}$ , and  $\hat{b}_{i,-\mathbf{p}_1-\mathbf{p}_2}$ , respectively.

The total particle number  $N$  and atomic number difference  $\delta N$  are defined as below:

$$N_1 + N_2 + 2N_M = N, \quad N_1 - N_2 = \delta N, \quad (3)$$

where we use  $N_{1,2} = \int d^3r \langle \hat{\psi}_{1,2}^\dagger \hat{\psi}_{1,2} \rangle$  and  $N_M = \sum_{i=x,y,z} \int d^3r \langle \hat{\phi}_i^\dagger \hat{\phi}_i \rangle$  to denote the numbers of atoms and molecules, respectively. Here  $\langle \dots \rangle$  represents the average over the ground state.  $N$  and  $\delta N$  are conserved in our model, which correspond to the  $U_N(1)$  and  $[SU(2)/U_y(1)]$  symmetries.

### III. MEAN-FIELD INSTABILITY

As the foundation of beyond-mean-field study, we need to characterize the ground state at the mean-field level first. We use the mean fields  $\Psi_1 = \langle \hat{\psi}_1 \rangle$ ,  $\Psi_2 = \langle \hat{\psi}_2 \rangle$ , and  $\Phi_i = \langle \hat{\phi}_i \rangle$  to describe the atomic and molecular condensates. The mean-field ground state of a  $p$ -wave resonant Bose gas including considerable large intraspecies  $s$ -wave interaction has been systematically discussed before [16,17]. Three mean-field phases for the ground states: atomic (ASF), atomic-molecular (AMSF), and molecular (MSF) superfluid, are found. Typically, the atomic condensates carry finite momentum due to the  $p$ -wave interaction in the AMSF phase. Actually, the ground-state phase diagram of our model is similar to the case there. Due to the lack of intraspecies  $s$ -wave interaction (or due to weak intraspecies  $s$ -wave interaction) in our model, it is shown that such previously known types of ground state are unstable at the mean-field level.

As the typical feature of  $p$ -wave interaction, the atomic condensates generally carry finite momentum due to the shift of energy minimum in momentum space by the interaction terms [16,17]. Although a general description of atomic order parameters should be written as  $\Psi_1 = \sum_{\mathbf{Q}_n} \Psi_{1,\mathbf{Q}_n} e^{-i\mathbf{Q}_n \cdot \mathbf{r}}$  and  $\Psi_2 = \sum_{\mathbf{Q}_n} \Psi_{2,-\mathbf{Q}_n} e^{i\mathbf{Q}_n \cdot \mathbf{r}}$ , where  $\mathbf{Q}_n$  is the set of possible momentums, it is generally expected that the assumption  $\mathbf{Q}_n = \mathbf{Q}$  is sufficient to capture the qualitative picture of the ground state. That is, the order parameters can be taken as

$$\Psi_1 = \Psi_{1,\mathbf{Q}} e^{-i\mathbf{Q} \cdot \mathbf{r}}, \quad \Psi_2 = \Psi_{2,-\mathbf{Q}} e^{i\mathbf{Q} \cdot \mathbf{r}}. \quad (4)$$

TABLE II. Ground-state phases. Here we have three phases by setting different detuning. ASF, AMSF, and MSF are the atomic, atomic-molecular, and molecular condensate phases, respectively.

Phase	$\epsilon_0$	$n_M$	$n_1 = n_2$	$Q$	$\mu$	$Z$	$E_0/V$
ASF	$\epsilon_0 < -\frac{1}{2}\bar{g}^2 mn$	0	$\frac{1}{2}n$	0	0	0	0
AMSF	$-\frac{1}{2}\bar{g}^2 mn < \epsilon_0 < \frac{1}{2}\bar{g}^2 mn$	$\frac{1}{4}n + \frac{\epsilon_0}{2\bar{g}^2 m}$	$\frac{1}{4}n - \frac{\epsilon_0}{2\bar{g}^2 m}$	$-\bar{g}m\sqrt{\frac{1}{4}n + \frac{\epsilon_0}{2\bar{g}^2 m}}$	$-\frac{1}{8}\bar{g}^2 mn - \frac{1}{4}\epsilon_0$	0	$-\frac{1}{16\bar{g}^2 m}(\bar{g}^2 mn + 2\epsilon_0)^2$
MSF	$\epsilon_0 > \frac{1}{2}\bar{g}^2 mn$	$\frac{1}{2}n$	0	$-\frac{1}{\sqrt{2}}\bar{g}m\sqrt{n}$	$-\frac{1}{4}\bar{g}^2 mn$	0	$-\frac{1}{2}\epsilon_0 n$

Correspondingly, the molecular components are space independent, since the molecular fields only feel a homogeneous potential by atoms. Considering the symmetries of our model, we have the following ground-state ansatz:

$$\begin{aligned}\Psi &= \sqrt{n_A} e^{i\theta} e^{i(\theta_x \sigma_x + \theta_z \sigma_z)} \begin{pmatrix} \cos \chi_A e^{-i\mathbf{Q}\cdot\mathbf{r}} \\ \sin \chi_A e^{i\mathbf{Q}\cdot\mathbf{r}} \end{pmatrix}, \\ \mathbf{Q} &= e^{i\sum_{i=x,y,z} \bar{\theta}_i \lambda_i} \mathbf{Q}_0, \\ \Phi &= \sqrt{n_M} e^{i(2\theta + \theta_M)} e^{i\sum_{i=x,y,z} \bar{\theta}_i \lambda_i} \begin{pmatrix} \cos \chi_M \\ i \sin \chi_M \\ 0 \end{pmatrix},\end{aligned}\quad (5)$$

where  $\theta, \theta_M \in [0, 2\pi)$  are U(1) phases,  $\theta_{x,z} \in [0, 2\pi)$  are [SU(2)/U<sub>y</sub>(1)] spin-rotation angles,  $\theta_{x,y,z}$  are SO(3) rotation angles,  $\chi_A, \chi_M \in [0, 2\pi)$ ,  $\mathbf{Q}_0 = (Q_{0,x}, Q_{0,y}, Q_{0,z})^T$  is an arbitrary real three-dimensional vector, and  $n_A = (N_1 + N_2)/V$ ,  $n_M = N_M/V$  with system volume  $V$  are the total atomic density and molecular density, respectively.

Furthermore, we derive the free energy density by substituting the above ansatz (5) to the Hamiltonian density (1):

$$\begin{aligned}F/V &= \sum_{\sigma=1,2} \frac{Q^2}{2m} n_\sigma - \epsilon_0 n_M - \mu(n_1 + n_2 + 2n_M - n) \\ &+ \frac{\bar{g}}{2} n_A \sqrt{n_M} \sin 2\chi_A [e^{-i\theta_M} (\cos \chi_M, -i \sin \chi_M, 0) \\ &\cdot \mathbf{Q}_0 + \text{H.c.}] - Z(n_1 - n_2),\end{aligned}\quad (6)$$

where  $n_{1,2} = N_{1,2}/V$ , and  $\mu$  and  $Z$  are the Lagrange multipliers set for the conservations of the total particle number and atom-number difference. For simplicity, we only consider a nonpolarized situation in this paper, i.e.,  $n_1 = n_2 = n_A/2$ , and fix the total particle number. The free energy density does not depend on  $\theta, \theta_{x,z}, \bar{\theta}_{x,y,z}$ . To minimize the free energy, we obtain the optimal values for the parameters:  $\theta_M = 0$ ,  $\chi_A = \pi/4$ ,  $\chi_M = 0$ ,  $Q_{0,x} = |\mathbf{Q}|$ ,  $Q_{0,y,z} = 0$ , from which we can see that  $\Phi$  is real and parallel to  $\mathbf{Q}$  by setting  $\theta = 0$ . To be more convenient, we set  $\bar{\theta}_y = \pi/2$ ,  $\bar{\theta}_{x,z} = 0$  so that  $\mathbf{Q}$  and  $\Phi$  are aligned to the  $z$  direction. Without loss of generality, we choose  $\bar{g}$  to be negative. (If  $\bar{g} > 0$ ,  $\mathbf{Q}$  will be opposite to  $\Phi$ ; however, it gives us the same phases and LHY corrections as we obtain below). The Gross-Pitaevskii (GP) equations can be derived from the free-energy-density formula, and we obtain the optimized solutions to minimize the free energy.

Similar to previous literature [16,17], the ground-state phase diagram of our model is also divided into three phases for different detuning  $\epsilon_0$ , where the ground-state phases are listed in Table II. Here ASF refers to the atomic superfluid phase, where only atomic condensates exist. Note that there is no superfluidity here due to the absence of background

atom-atom interaction, where the name of phase is taken to be consistent only with previous convention [16,17]. AMSF refers to the atomic-molecular superfluid phase, where atom and molecular condensates are present in the same phase. MSF with only molecular condensate is the molecular superfluid phase.

In the ASF phase, the condensate in both atomic species stays stationary due to vanishing  $\mathbf{Q}$  and the two condensates do not interact. The atomic chemical potential remains zero. In the AMSF phase, the rotation and time-reversal symmetries are all broken due to the finite-momentum condensates. The SO(3) rotation symmetry is spontaneously broken into SO(2) symmetry. In the MSF phase, although the density of the atomic condensates is zero, we still have nonzero  $\mathbf{Q}$ . This results in an MSF excitation spectrum translated in momentum space by  $\mathbf{Q}$ , as we will see in Sec. IV.

From Table II, we can also find the total energy  $E_0$  is proportional to particle number  $N = nV$  in phases ASF and MSF, which is due to the lack of background atom-atom and molecule-molecule interactions in these phases, respectively. It means the total energy  $E_0$  is constant, such that the ground state is stable, for a system with fixed total particle number. However, we can find it is energetically favorable to increase the density  $n$  to reach a lower total energy  $E_0$  in the AMSF phase. This implies that in this phase the mean-field ground state is unstable and tends to collapse into a state with smaller volume but large particle density when the total particle number is fixed. The instability of the ground state in the AMSF phase also manifests itself in the fact that the excitation mode becomes complex in the long-wavelength limit  $k \rightarrow 0$  [18]. It will be shown that the ground state collapses into a small droplet after considering LHY correction [13]. In order to calculate this correction, we need to analyze the Bogoliubov excitation spectrum first.

#### IV. BOGOLIUBOV EXCITATION SPECTRUM

We will study the Bogoliubov excitation spectrum in this section. Following Bogoliubov's theory [19,20], we expand the atomic and molecular fields around the ground-state mean fields,

$$\hat{\psi}_\sigma = \Psi_\sigma + \delta\hat{\psi}_\sigma, \quad \hat{\phi}_i = \Phi_i + \delta\hat{\phi}_i, \quad (7)$$

with the fluctuation fields  $\delta\hat{\psi}_\sigma$  and  $\delta\hat{\phi}_i$ . For convenience, we furthermore expand  $\delta\hat{\psi}_\sigma$  and  $\delta\hat{\phi}_i$  with the Fourier transformation

$$\delta\hat{\psi}_\sigma = \frac{1}{\sqrt{V}} \sum_{\mathbf{k}} \delta\hat{a}_{\sigma,\mathbf{k}} e^{-i\mathbf{k}\cdot\mathbf{r}}, \quad \delta\hat{\phi}_i = \frac{1}{\sqrt{V}} \sum_{\mathbf{k}} \delta\hat{b}_{i,\mathbf{k}} e^{-i\mathbf{k}\cdot\mathbf{r}}, \quad (8)$$

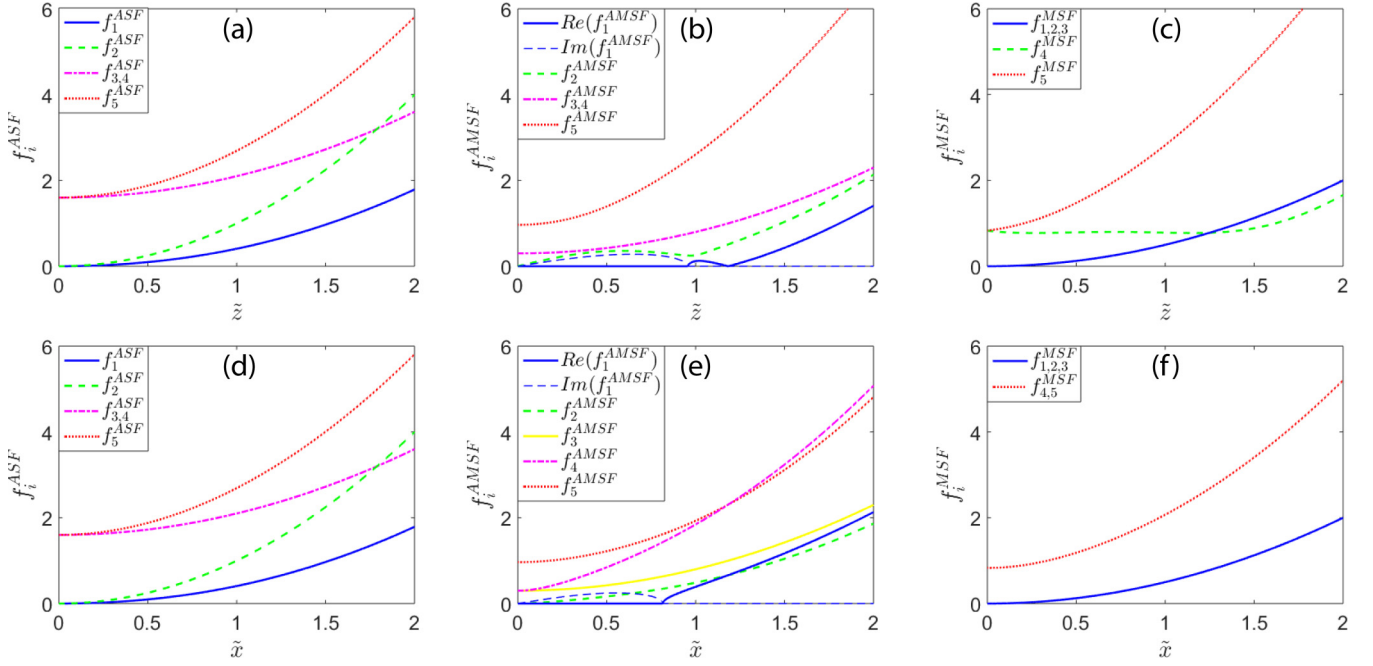


FIG. 1. Schematic plot of dimensionless function  $f_j$  for  $\Delta = -0.4$  (a, d),  $\Delta = 0.1$  (b, e), and  $\Delta = 0.4$  (c, f), which is inside the ASF, AMSF, and MSF phases, respectively. We find that the low-energy modes become imaginary in the AMSF phase, which arises from the instability of the mean-field ground state. Here  $\tilde{r} = \sqrt{\tilde{x}^2 + \tilde{y}^2 + \tilde{z}^2}$  represents the distance from the momentum-space origin.

where  $\delta\hat{a}_{\sigma,\mathbf{k}}$  and  $\delta\hat{b}_{i,\mathbf{k}}$  are the corresponding quantum fluctuation fields in momentum space. Substituting Eqs. (7) and (8) into Eq. (1) and keeping only the second-order terms (the first-order terms vanish due to the saddle-point solution and higher-order terms will be neglected), we can derive the Bogoliubov Hamiltonian. The Bogoliubov excitation spectrum can be extracted by diagonalizing the Bogoliubov Hamiltonian.

### A. ASF phase

This phase has only atomic condensates, i.e.,  $n_1 = n_2 = n/2$ ,  $n_M = 0$ , and the zero atomic condensates momentum  $\mathbf{Q} = 0$ . The Bogoliubov Hamiltonian can be written as

$$H_f = \frac{1}{2} \sum_{\mathbf{k}} \left\{ \sum_{\sigma=1,2} \varepsilon_{\sigma,\mathbf{k}+\mathbf{Q}_\sigma} \delta\hat{a}_{\sigma,\mathbf{k}+\mathbf{Q}_\sigma}^\dagger \delta\hat{a}_{\sigma,\mathbf{k}+\mathbf{Q}_\sigma} + \sum_i \omega_{i,\mathbf{k}} \delta\hat{b}_{i,\mathbf{k}}^\dagger \delta\hat{b}_{i,\mathbf{k}} - 2 \sum_{\sigma,i} \alpha_{i,\bar{\sigma},\mathbf{k}} \delta\hat{b}_{i,\mathbf{k}}^\dagger \delta\hat{a}_{\sigma,\mathbf{k}+\mathbf{Q}_\sigma} + \text{H.c.} \right\}, \quad (9)$$

where  $\bar{\sigma} = 3 - \sigma$ ,  $\sigma = 1, 2$ ,  $\mathbf{Q}_1 = -\mathbf{Q}_2 = \mathbf{Q}$ , and the parameters are given as

$$\varepsilon_{\sigma,\mathbf{k}} = \epsilon_k = \frac{k^2}{2m}, \quad \omega_{i,\mathbf{k}} = \frac{1}{2} \epsilon_k + \frac{1}{2} \bar{g}^2 mn, \\ \alpha_{i,\sigma,\mathbf{k}} = (-1)^\sigma \frac{1}{2\sqrt{2}} \bar{g} \sqrt{nk_i}. \quad (10)$$

The corresponding Bogoliubov excitation spectrum is given by

$$E_j^{\text{ASF}} = \frac{1}{4} \bar{g}^2 mn f_j^{\text{ASF}}(\tilde{x}, \tilde{y}, \tilde{z}), \quad j = 1, \dots, 5, \quad (11)$$

where  $f_j^{\text{ASF}}$  is a dimensionless function, and the dimensionless variables  $\tilde{x} = \frac{k_x}{\bar{g}m\sqrt{n}}$ ,  $\tilde{y} = \frac{k_y}{\bar{g}m\sqrt{n}}$ ,  $\tilde{z} = \frac{k_z}{\bar{g}m\sqrt{n}}$ .

We show  $f_j^{\text{ASF}}$  along the radial direction in Figs. 1(a) and 1(d). The spectrum is symmetric in all directions and has two gapless atomic modes. The quadratic dispersions of gapless mode are due to the absence of atom-atom interaction.

### B. AMSF phase

In the AMSF phase, particles are condensed into both the atomic and molecular channels, and the atomic condensates carry opposite finite momenta. The directions of atomic momentum  $\mathbf{Q}$  and the molecular condensates order parameter  $\Phi = (\Phi_x, \Phi_y, \Phi_z)$  are parallel in the mean-field ground state, where the direction of  $\Phi$  is defined by the three spatial components. For convenience, we build the coordinate so that this direction is aligned along the  $z$  axis. The Bogoliubov Hamiltonian is written as

$$H_f = \sum_{\mathbf{k}} \left\{ \sum_{\sigma=1,2} \frac{1}{2} \varepsilon_{\sigma,\mathbf{k}+\mathbf{Q}_\sigma} \delta\hat{a}_{\sigma,\mathbf{k}+\mathbf{Q}_\sigma}^\dagger \delta\hat{a}_{\sigma,\mathbf{k}+\mathbf{Q}_\sigma} + \sum_i \frac{1}{2} \omega_{i,\mathbf{k}} \delta\hat{b}_{i,\mathbf{k}}^\dagger \delta\hat{b}_{i,\mathbf{k}} + \mathbf{t}_{\mathbf{k}+\mathbf{Q}} \delta\hat{a}_{1,\mathbf{k}+\mathbf{Q}} \delta\hat{a}_{2,-\mathbf{k}-\mathbf{Q}} - \sum_{\sigma,i} \alpha_{i,\bar{\sigma},\mathbf{k}} \delta\hat{b}_{i,\mathbf{k}}^\dagger \delta\hat{a}_{\sigma,\mathbf{k}+\mathbf{Q}_\sigma} + \text{H.c.} \right\}, \quad (12)$$

where the parameters are given by

$$\begin{aligned} \varepsilon_{\sigma,\mathbf{k}} &= \epsilon_k + \frac{1}{8}\bar{g}^2 mn + \frac{1}{4}\epsilon_0, & \omega_{i,\mathbf{k}} &= \frac{1}{2}\epsilon_k + \frac{1}{4}\bar{g}^2 mn - \frac{1}{2}\epsilon_0, \\ t_{\mathbf{k}} &= -\bar{g} \sum_i \Phi_i^* k_i, & \alpha_{i,\bar{\sigma},\mathbf{k}} &= \pm \bar{g} \sqrt{n_\sigma} (Q_{\sigma,i} - k_i/2), \end{aligned} \quad (13)$$

with  $\epsilon_k = \frac{k^2}{2m}$ ,  $\sigma = 1, 2$  (correspondingly  $\bar{\sigma} = 2, 1$ ),  $\mathbf{Q}_1 = \mathbf{Q}$ , and  $\mathbf{Q}_2 = -\mathbf{Q}$ . The Bogoliubov excitation spectrum can be written as

$$E_j^{\text{AMSF}} = \frac{1}{4}\bar{g}^2 mn f_j^{\text{AMSF}}(\tilde{x}, \tilde{y}, \tilde{z}, \Delta), \quad j = 1, \dots, 5, \quad (14)$$

where  $f_j^{\text{AMSF}}$  is a dimensionless function and  $\Delta = \frac{\epsilon_0}{2\bar{g}^2 mn}$  is the dimensionless detuning.

The schematic plots of  $f_j^{\text{AMSF}}$  are shown in Figs. 1(b) and 1(e) along the  $z$  and  $x$  directions, respectively. As we can see from the two figures, the blue-dashed curve shows an imaginary mode consistent with the instability of the mean-field ground state [18], which is absent when the ground state is stable [16,17]. Actually, the true ground state is lost due to the homogeneous assumption (the system with a finite particle number will collapse into a droplet shape that breaks the spatial translation symmetry) and the absence of LHY correction. On the other hand, the inverse of the largest momentum carried by imaginary modes is expected to be comparable with the size of the droplet [18]. The minima on the blue-solid curve in Fig. 1(b) corresponds to the nonvanishing momentum  $2\mathbf{Q}$  in the AMSF phase, where the atomic condensates locate. That the spectrum softens to zero at  $k_z = 2Q$  implies our ansatz correctly captures the feature of the ground state.

### C. MSF phase

In this phase, we have  $n_M = n/2$  and  $n_1 = n_2 = 0$ . The Bogoliubov Hamiltonian is given as

$$\begin{aligned} H_f &= \sum_{\mathbf{k}} \left\{ \sum_{\sigma=1,2} \frac{1}{2} \varepsilon_{\sigma,\mathbf{k}+\mathbf{Q}_\sigma} \delta \hat{a}_{\sigma,\mathbf{k}+\mathbf{Q}_\sigma}^\dagger \delta \hat{a}_{\sigma,\mathbf{k}+\mathbf{Q}_\sigma} \right. \\ &\quad + t_{\mathbf{k}+\mathbf{Q}} \delta \hat{a}_{1,\mathbf{k}+\mathbf{Q}} \delta \hat{a}_{2,-\mathbf{k}-\mathbf{Q}} \\ &\quad \left. + \sum_i \frac{1}{2} \omega_{i,\mathbf{k}} \delta \hat{a}_{i,\mathbf{k}}^\dagger \delta \hat{a}_{i,\mathbf{k}} + \text{H.c.} \right\}, \end{aligned} \quad (15)$$

where  $\varepsilon_{\sigma,\mathbf{k}} = \epsilon_k + \frac{1}{4}\bar{g}^2 mn$ ,  $\omega_{i,\mathbf{k}} = \frac{1}{2}\epsilon_k$ , and  $t_{\mathbf{k}} = -\bar{g} \sum_i \Phi_i^* k_i$ .

Fortunately, we can derive analytical formulas for the excitation modes in this phase, i.e.,

$$\begin{aligned} E_{1,2,3}^{\text{MSF}} &= \frac{1}{8}\bar{g}^2 mn \tilde{r}^2, \\ E_4^{\text{MSF}} &= \frac{1}{4}\bar{g}^2 mn \sqrt{(\tilde{r}^2 + 2\Delta - \frac{1}{2})(\tilde{r}^2 - 2\sqrt{2}\tilde{r} \cos \gamma + 2\Delta + \frac{3}{2})}, \\ E_5^{\text{MSF}} &= \frac{1}{4}\bar{g}^2 mn \sqrt{(\tilde{r}^2 + 2\Delta - \frac{1}{2})(\tilde{r}^2 + 2\sqrt{2}\tilde{r} \cos \gamma + 2\Delta + \frac{3}{2})}, \end{aligned} \quad (16)$$

where  $\tilde{r}^2 = (k_x^2 + k_y^2 + k_z^2)/\bar{g}^2 m^2 n$ , and  $\gamma$  is the angle between the  $z$  axis and unit vector  $\hat{\mathbf{k}}$  as we have aligned  $\hat{\mathbf{Q}}$  along  $z$ . Similar to what we defined in the ASF and AMSF phases, we

rewrite the excitation modes in this formula

$$E_j^{\text{MSF}} = \frac{1}{4}\bar{g}^2 mn f_j^{\text{MSF}}(\tilde{x}, \tilde{y}, \tilde{z}, \Delta), \quad j = 1, \dots, 5. \quad (17)$$

Figures 1(c) and 1(f) are the corresponding  $f_j^{\text{MSF}}$  along the  $z$  and  $x$  directions. In Fig. 1(c), the red dotted and green dashed curves are the two atom modes, respectively, and the minima on green dashed curve corresponds to the nonvanishing momentum  $2\mathbf{Q}$ . The blue curve denotes the triply degenerated molecule modes. In Fig. 1(f), the red curve denotes the doubly degenerated atom modes, and the blue curve denotes the triply degenerated molecule modes.

### V. LHY CORRECTION

The LHY correction is the leading-order correction of quantum fluctuation. It is composed of Bogoliubov excitation energies, commutation energies which appear due to the commutation relations of the Nambu basis, and energy correction due to the interaction renormalization. Here the interaction renormalization is employed to remove the energy divergence arising in collecting the energy of quantum fluctuation [13]. Let us review the renormalization procedure before going ahead.

To remove the divergence that appears in the calculation of LHY correction, we need to renormalize the interaction parameter  $\bar{g}$  and detuning  $\epsilon_0$  [13,18]. The two-body T matrix for  $p$ -wave interaction is given by [21]

$$\begin{aligned} -iT_{\mathbf{k},\mathbf{k}'}^{(l_z)}(k) &= D^{(0)}(k)(-i\bar{g})^2 k^2 Y_{1,l_z}(\hat{\mathbf{k}}) Y_{1,l_z}^*(\hat{\mathbf{k}}') \\ &\quad + D^{(0)2}(k)(-i\bar{g})^4 2\Pi_{l_z}(k) k^2 Y_{1,l_z}(\hat{\mathbf{k}}) Y_{1,l_z}^*(\hat{\mathbf{k}}') + \dots \\ &= D(k)(-i\bar{g})^2 k^2 Y_{1,l_z}(\hat{\mathbf{k}}) Y_{1,l_z}^*(\hat{\mathbf{k}}'), \end{aligned} \quad (18)$$

where the index  $l_z$  denotes different interacting channels  $l_z = -1, 0, 1$ .  $Y_{1,l_z}(\hat{\mathbf{k}})$  is the  $l_z$ th channel of the first-order spherical harmonics.  $D^{(0)}(k)$  is the  $p$ -wave scattering propagator, and  $\Pi_{l_z}(k)$  is the polarization bubble for channel  $l_z$ , which are given by

$$D^{(0)}(k) = \frac{i}{k^2/m + \epsilon_0 + i0^+} \quad (19)$$

and

$$\Pi_{l_z}(k) = \int \frac{d^3 p}{(2\pi)^3} \frac{ip^2 |Y_{1,l_z}(\hat{\mathbf{p}})|^2}{k^2/m - p^2/m + i0^+}. \quad (20)$$

Using Eq. (18), we yield

$$D^{-1}(k) = [D^{(0)}(k)]^{-1} - (-i\bar{g})^2 \Pi_{l_z}(k). \quad (21)$$

Comparing the  $k^0$  term and  $k^2$  term on both sides of Eq. (21), we obtain the renormalization relations [22]

$$\frac{\tilde{\epsilon}_0}{\tilde{g}^2} = \frac{\epsilon_0}{\bar{g}^2} + \int \frac{d^3 p}{(2\pi)^3} m |Y_{1,l_z}(\hat{\mathbf{p}})|^2 \quad (22)$$

and

$$\frac{1}{\tilde{g}^2} = \frac{1}{\bar{g}^2} - \int \frac{d^3 p}{(2\pi)^3} m^2 \frac{|Y_{1,l_z}(\hat{\mathbf{p}})|^2}{p^2}, \quad (23)$$

where  $\tilde{\epsilon}_0$  and  $\tilde{g}$  are the renormalized detuning and  $p$ -wave interacting strength, respectively.

Applying these renormalization relations into the ground-state energy in different phases, one obtains the renormalized mean-field ground-state energies

$$E_{0,r}^{\text{ASF}}/V = 0, \quad (24)$$

$$E_{0,r}^{\text{AMSF}}/V = \int \frac{d^3k}{(2\pi)^3} \left( \frac{1}{12} \bar{g}^2 mn + \frac{1}{6} \epsilon_0 + \frac{\bar{g}^4 m^2 n^2 - 4\epsilon_0^2}{72k^2} \right), \quad (25)$$

and

$$E_{0,r}^{\text{MSF}}/V = \int \frac{d^3k}{(2\pi)^3} \left( \frac{1}{6} \bar{g}^2 mn + \frac{\bar{g}^2 mn - 2\epsilon_0}{12k^2} \right). \quad (26)$$

From the analysis of the Bogoliubov spectrum and interaction renormalization, we obtain the LHY correction densities in different phases,

$$E_{\text{LHY}}^{\text{ASF}}/V = -\bar{g}^5 m^4 n^{2.5} \int \frac{d^3\tilde{r}}{(2\pi)^3} \left( \sum_{j=1}^5 \frac{1}{4} f_j^{\text{ASF}} - \frac{7}{8} \tilde{r}^2 + 3\Delta \right), \quad (27)$$

$$E_{\text{LHY}}^{\text{AMSF}}/V = -\bar{g}^5 m^4 n^{2.5} \int \frac{d^3\tilde{r}}{(2\pi)^3} \left( \sum_{j=1}^5 \frac{1}{4} f_j^{\text{AMSF}} - \frac{7}{8} \tilde{r}^2 - \frac{13}{24} + \frac{5}{6} \Delta + \frac{1 - 16\Delta^2}{72\tilde{r}^2} \right), \quad (28)$$

and

$$E_{\text{LHY}}^{\text{MSF}}/V = -\bar{g}^5 m^4 n^{2.5} \int \frac{d^3\tilde{r}}{(2\pi)^3} \left( \sum_{j=1}^5 \frac{1}{4} f_j^{\text{MSF}} - \frac{7}{8} \tilde{r}^2 - \frac{1}{3} + \frac{1 - 4\Delta}{12\tilde{r}^2} \right). \quad (29)$$

Unlike the AMSF and MSF phases, there is no particle-hole coupling as presented in Eq. (9) in the ASF phase, which results in the cancellation between the total excitation energies and the commutation energies in LHY calculation. As a proof to this inference, we find Eq. (27) shows result  $E_{\text{LHY}}^{\text{ASF}} = 0$  numerically. Combining the mean-field ground-state energy densities and LHY-corrected energy densities yields the total ground-state energy density  $E_g/V = E_0/V + E_{\text{LHY}}/V$  for different phases as follows:

$$E_g^{\text{ASF}}/V = 0, \quad (30)$$

$$E_g^{\text{AMSF}}/V = -\bar{g}^5 m^4 n^{2.5} F(\Delta) - \frac{1}{16} \bar{g}^2 mn^2 - \frac{1}{4} \epsilon_0 n - \frac{1}{4} \frac{\epsilon_0^2}{\bar{g}^2 m}, \quad (31)$$

and

$$E_g^{\text{MSF}}/V = -\bar{g}^5 m^4 n^{2.5} F(\Delta) - \frac{1}{2} n \epsilon_0, \quad (32)$$

where  $F(\Delta)$  is depicted in Fig. 2 numerically.

We plot the total energy density versus particle density for different detuning in Fig. 3. As we can see, for  $\epsilon_0 > 0$ , the minimum energy density is well defined and lies in the

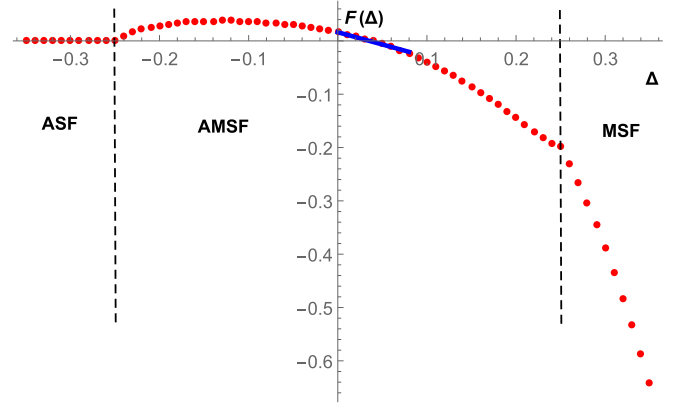


FIG. 2. Schematic plot of  $F(\Delta)$ . The blue solid line is a linearized approximation for the regime with a stabilized particle number density.

AMSF phase. It implies that there exists a self-stabilized state at around the minimum. If the particle number is finite, it forms a quantum droplet [1]. We also depict the dependence between the particle density of the self-stabilized state  $n_s$  and the detuning  $\epsilon_0$  in Fig. 4. It is shown that the stabilized density is almost linearly proportional to  $\epsilon_0$ . However, if  $\epsilon_0 < 0$ , the energy density is degenerated inside the ASF phase, but it can be broken by introducing an atom-atom  $s$ -wave interaction. Typically, the atom-atom  $s$ -wave interaction is repulsive and the corresponding LHY correction is also positive [13]. Therefore, the lowest energy density lies at  $n = 0$  inside ASF phase. For this reason, we do not expect a self-stabilized state when the detuning  $\epsilon_0 < 0$ .

The diluteness of  $p$ -wave interacting gas can be characterized by the product between the particle density and the scattering volume  $v_p$  [22,23], i.e.,  $nv_p = \bar{g}^2 mn / (16\pi^2 \epsilon_0)$ . Therefore, we can rewrite the ground-state energy given by mean-field theory (MFT) and the LHY correction in terms of the diluteness as

$$E_{\text{AMSF}}^{\text{MFT}}/V = -\frac{\epsilon_0^2}{64\bar{g}^2 m} (32\pi^2 nv_p + 4)^2, \quad (33)$$

$$E_{\text{MSF}}^{\text{MFT}}/V = -\frac{\epsilon_0^2}{4\bar{g}^2 m} 32\pi^2 nv_p, \quad (34)$$

and

$$E^{\text{LHY}}/V = m^{1.5} (\epsilon_0/2)^{2.5} (32\pi^2 nv_p)^{2.5} F\left(\frac{1}{32\pi^2 nv_p}\right). \quad (35)$$

The diluteness of the self-stabilized state with respect to detuning is shown in Fig. 5. As detuning approaches zero, the diluteness tends to diverge, which may indicate that higher-order corrections besides MFT and LHY are needed. But for a large detuning regime, the mixture is dilute, so it is reasonable to characterize our model with only first-order beyond-mean-field calculation.

## VI. QUANTUM DROPLETS

According to the above analysis, we find the mean-field collapsing state becomes self-stabilized after considering beyond-mean-field correction. This self-stabilized state forms

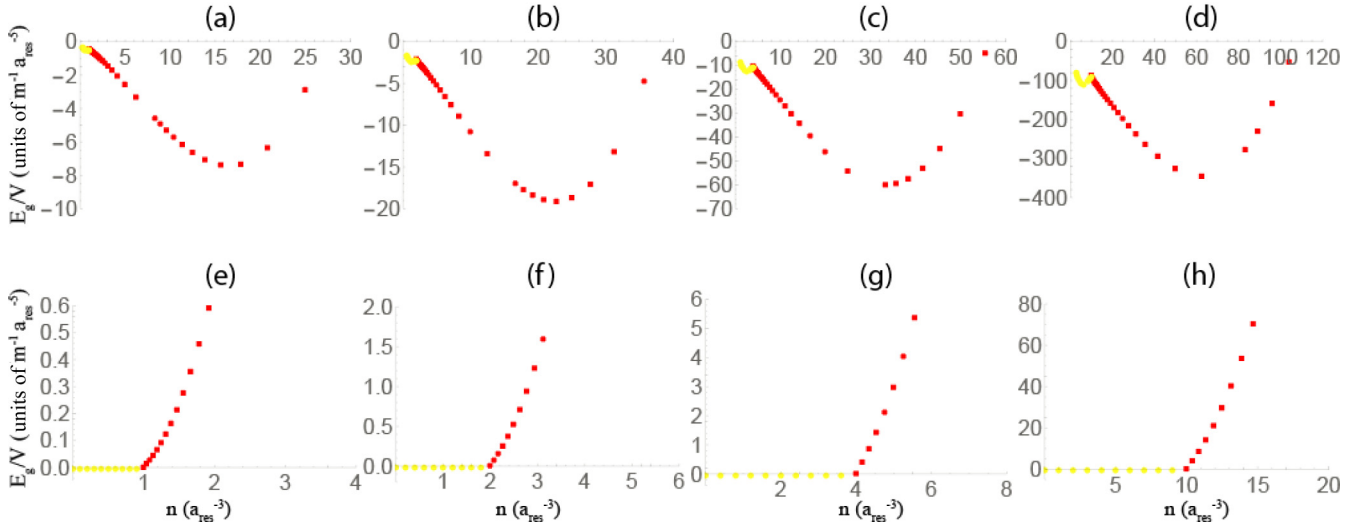


FIG. 3. Total ground-state energy density vs total number density for different detuning:  $\epsilon_0 m a_{\text{res}}^2 = 0.5$  (a), 1 (b), 2 (c), 5 (d),  $-0.5$  (e),  $-1$  (f),  $-2$  (g), and  $-5$  (h). In subfigures with  $\epsilon_0 > 0$ , the yellow circle (red square) dots represent the energies in MSF (AMSF) phase. The minimum energy density is presented with a finite number density after we introduce the LHY correction and lies in the AMSF phase. In subfigures with  $\epsilon_0 < 0$ , the yellow circle (red square) dots represent the energies in ASF (AMSF) phase. To emphasize the dominance of  $p$ -wave interaction, we choose  $a_{\text{res}} = 10^3 a_0$  with the Bohr radius  $a_0$  as the unit of length, which is typically far larger than the background scattering length. We set the Planck constant  $\hbar$  as 1 for convenience.

a quantum droplet when the particle number is finite [1]. To figure out the density distribution of the quantum droplet, we will derive an effective theory to characterize the density profile. Here we employ the function  $\xi(\mathbf{r})$  to characterize the droplet density profile. If the system size is infinite, we have the solution  $\xi(\mathbf{r}) = 1$ , as it should be a uniform gas. However, if the system size is finite, the density profile will be inhomogeneous.

As a qualitative analysis, we will take the local density approximation (LDA). With this approximation, the order parameters can be rewritten as [18]

$$\Psi_1 = \Psi_{1,\mathbf{Q}} e^{-i\mathbf{Q}\cdot\mathbf{r}}, \quad \Psi_2 = \Psi_{2,-\mathbf{Q}} e^{i\mathbf{Q}\cdot\mathbf{r}}, \quad (36)$$

and  $\Phi = \sqrt{n_{s,M}} \xi(\mathbf{r}) \hat{\mathbf{z}}$ , where

$$\Psi_{1,\mathbf{Q}} = \sqrt{n_{s,1}} \xi(\mathbf{r}), \quad \Psi_{2,-\mathbf{Q}} = \sqrt{n_{s,2}} \xi(\mathbf{r}). \quad (37)$$

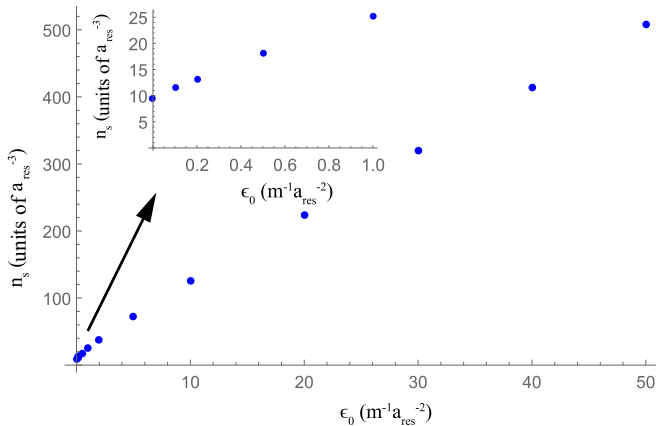


FIG. 4. The stabilized density  $n_s$  vs detuning  $\epsilon_0$ . The stabilized density  $n_s$  is almost proportional to detuning  $\epsilon_0$  linearly. As  $\epsilon_0$  becomes larger,  $\Delta_s = \frac{\epsilon_0}{2g^2 m_s}$  converges to  $\sim 0.08$ .

$n_{s,\{1,2,M\}}$  are the densities that correspond to the minimum of  $E_g/V$  as shown in Fig. 3. Here we have chosen the  $\hat{\mathbf{z}}$  direction due to the spontaneous breaking of the  $SO(3)$  rotation symmetry by  $\mathbf{Q} = -\bar{g}m\sqrt{n_{s,M}}\xi(\mathbf{r})\hat{\mathbf{z}}$ .

To access the analytical form of effective Hamiltonian, an approximative form of  $F(\Delta)$  at around the stable point is considered. For  $\epsilon_0 > 0$ , we find a linearized formula for  $F(\Delta)$  which captures its behavior at around the minimum energy density inside the AMSF phase ( $0 < \Delta < \approx 0.08$ ) [see Fig. 2]. It is written as

$$F(\Delta) \approx -0.460333\Delta + 0.01624807. \quad (38)$$

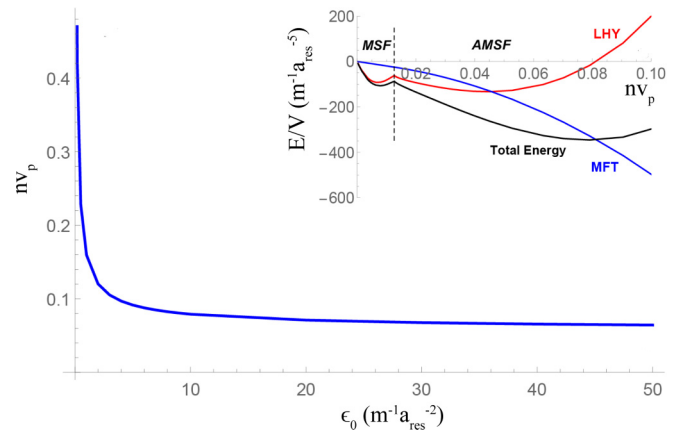


FIG. 5. Relation between diluteness and the detuning. As detuning approaches zero, the diluteness tends to diverge, which may indicate that higher-order corrections besides MFT and LHY are needed. But for a large detuning regime, the mixture is dilute, so it is reasonable to characterize our model with only first-order beyond-mean-field calculation. The inset shows the energy comparison for different diluteness, as we set  $\epsilon_0 m a_{\text{res}}^2 = 5$ . The lowest total energy is ensured to appear in the dilute regime.

According to Eq. (31), the approximated total ground-state energy in the AMSF phase is given by

$$E_g^{\text{AMSF}}/V = -\frac{1}{16}\bar{g}^2 m n_s^2 - \frac{1}{4}\epsilon_0 n_s - \frac{1}{4}\frac{\epsilon_0^2}{\bar{g}^2 m} - 0.01625\bar{g}^5 m^4 n_s^{2.5} + 0.2302\epsilon_0 \bar{g}^3 m^3 n_s^{1.5}. \quad (39)$$

Furthermore, by substituting Eqs. (36) and (37) to Eq. (39) along with the kinetic energy, we derive the effective Hamiltonian

$$\begin{aligned} \mathcal{H}_{\text{eff}} = \bar{g}^2 m n_s^2 \left\{ \left[ \frac{1}{\bar{g}^2 m^2 n_s} \left( \frac{3}{4}\Delta - \frac{5}{16} \right) + \left( \Delta^2 - \frac{1}{16} \right) z^2 \xi^2 \right] \xi \nabla^2 \xi \right. \\ \left. - \left( 2\Delta^2 + \frac{1}{2}\Delta \right) \xi^2 + 0.460333\Delta \bar{g}^3 m^3 \sqrt{n_s} \xi^3 \right. \\ \left. + \left( \Delta^2 - \frac{1}{16} \right) \xi^4 - 0.01625\bar{g}^3 m^3 \sqrt{n_s} \xi^5 \right\} \quad (40) \end{aligned}$$

The chemical potential  $\tilde{\mu}$  is fixed by the normalization condition  $\int d^3r |\xi|^2 = N/n_s$ , where  $N$  is the total number of particles and  $n_s$  is the stabilized total density. The profile function  $\xi(\mathbf{r})$  is determined by the GP equation

$$\begin{aligned} \tilde{\mu} \xi^2 = \bar{g}^2 m n_s^2 \left\{ \left[ \frac{1}{\bar{g}^2 m^2 n_s} \left( \frac{3}{4}\Delta - \frac{5}{16} \right) + 2 \left( \Delta^2 - \frac{1}{16} \right) z^2 \xi^2 \right] \xi \nabla^2 \xi \right. \\ \left. - \left( 2\Delta^2 + \frac{1}{2}\Delta \right) \xi^2 + 0.690501\Delta \bar{g}^3 m^3 \sqrt{n_s} \xi^3 \right. \\ \left. + 2 \left( \Delta^2 - \frac{1}{16} \right) \xi^4 - 0.0460202\bar{g}^3 m^3 \sqrt{n_s} \xi^5 \right\}, \quad (41) \end{aligned}$$

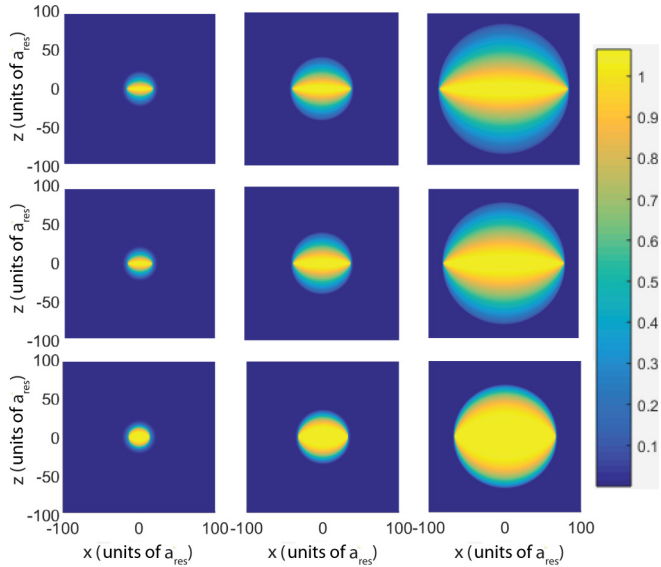


FIG. 6. Density profile of the droplet. The background color represents  $\xi = \sqrt{n(\mathbf{r})/n_s}$ , where  $n(\mathbf{r})$  is density at different locations and  $n_s$  is the stabilized density. The  $x$  axis and  $y$  axis for each subfigure label the  $x$  direction and  $z$  direction in real space. The detunings from the top row to the bottom row are  $\epsilon_0 m a_{\text{res}}^2 = 0.5, 5, 50$ , respectively. The normalization factors for  $\xi$  from the left column to the right column are  $N/(n_s a_{\text{res}}^3) = 10^4, 10^5, 10^6$ , respectively. When the particle number grows large enough with  $n_s$  fixed, it clearly breaks  $\text{SO}(3)$  symmetry. As the detuning grows smaller and deep inside the AMSF phase, the droplet is more and more reduced along the  $z$  axis.

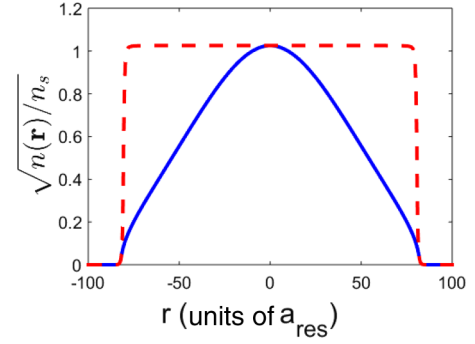


FIG. 7. Density profile on the centered lines along the  $x$  and  $z$  directions inside the droplet under condition  $\epsilon_0 m a_{\text{res}}^2 = 0.5$  and  $N/(n_s a_{\text{res}}^3) = 10^6$ . The red dashed curve is the centered line along the  $x$  direction and the blue solid curve is along the  $z$  direction. The value on the plateau is almost constant and close to 1.025. If the system size is increased, the height of the plateau will be closer to 1.

which is derived by minimizing the effective Hamiltonian.

The above GP equation is solved numerically by using the imaginary time evolution method. The solutions for different detuning and particle numbers are shown in Fig. 6. We can find that the quantum droplet is typically suppressed in the  $z$  direction. The degrees of suppression decrease for a larger  $\epsilon_0$ . Hence the droplet looks like a pancake when  $N/n_s$  is large enough but  $\epsilon_0$  is small (see the upper-right subfigure of Fig. 6). We also show the section of the solution where  $\epsilon_0 m a_{\text{res}}^2 = 0.5$ ,  $N/(n_s a_{\text{res}}^3) = 10^6$  in Fig. 7. The density is found to suddenly fall to zero in the horizontal directions ( $x$  or  $y$  directions) while gently decreasing to zero in the  $z$  direction. Except for the boundary regime, the profile varies smoothly everywhere, which implies that LDA could qualitatively catch the features of the quantum droplet here. In fact, the anisotropy of the quantum droplet arises from the spontaneous breaking of  $\text{SO}(3)$  rotation symmetry by finite-momentum atomic condensates. It is intrinsically different from the anisotropic quantum droplets in the presence of dipolar interaction [6–9] or spin-orbit coupling [12], where the anisotropy arises from external fields. As we can see, the value on the plateau remains almost constant and close to 1, which will be exactly 1 when the system size goes to infinity. Another special feature of the quantum droplet here is that the atomic components carry finite momentums due to the breaking of time-reversal symmetry.

## VII. BACKGROUND S-WAVE INTERACTIONS

Previously we mainly focused on the case without background interactions. In the presence of the background  $s$ -wave interactions, which are characterized by

$$\begin{aligned} \hat{V}_{bg} = g_1 \hat{\psi}_1^\dagger \hat{\psi}_1^\dagger \hat{\psi}_1 \hat{\psi}_1 + g_2 \hat{\psi}_2^\dagger \hat{\psi}_2^\dagger \hat{\psi}_2 \hat{\psi}_2 + g_{12} \hat{\psi}_1^\dagger \hat{\psi}_2^\dagger \hat{\psi}_2 \hat{\psi}_1 \\ + g_{mm}^{(1)} \sum_{i,j=x,y,z} \hat{\phi}_i^\dagger \hat{\phi}_j^\dagger \hat{\phi}_j \hat{\phi}_i + g_{mm}^{(2)} \sum_{i,j=x,y,z} \hat{\phi}_i^\dagger \hat{\phi}_i^\dagger \hat{\phi}_j \hat{\phi}_j \\ + g_{am} \sum_{\sigma=1,2} \sum_{i=x,y,z} \hat{\psi}_\sigma^\dagger \hat{\phi}_i^\dagger \hat{\phi}_i \hat{\psi}_\sigma, \quad (42) \end{aligned}$$

where  $g_1$ ,  $g_2$ , and  $g_{12}$  ( $g_{mm}^{(1)}$  and  $g_{mm}^{(2)}$ ) are the atom-atom (molecule-molecule) interaction coefficients and  $g_{am}$  is the atom-molecule interaction coefficient, the mean-field ground-state energy in the AMSF phase (taking the polar molecular state [16,17] as example) takes the form

$$\begin{aligned} \frac{E_0}{V} = & [-4\epsilon_0^2(g_{aa} - 3g_{am} + 2g_{mm} + \bar{g}^2 m) \\ & - 4\epsilon_0 n(2g_{aa} - 2g_{am} + \bar{g}^2 m) \\ & \times (g_{aa} - 3g_{am} + 2g_{mm} + \bar{g}^2 m) \\ & + (4g_{aa}^2 g_{am} + (3g_{am} - 2g_{mm} - \bar{g}^2 m)(-2g_{am} + \bar{g}^2 m)^2 \\ & - g_{aa}(12g_{am}^2 - 4g_{mm}^2 - 8g_{am}\bar{g}^2 m + \bar{g}^4 m^2))n^2] \\ & / [16(g_{aa} - 2g_{am} + g_{mm} + \bar{g}^2 m)^2]. \end{aligned} \quad (43)$$

Here  $g_{aa} = g_1 + g_2 + g_{12}$  and  $g_{mm} = g_{mm}^{(1)} + g_{mm}^{(2)}$ . In order to capture the profile of a quantum droplet with finite particle number, we consider the ground-state energy with the canonical condition in this paper instead of the grand-canonical condition in Refs. [16,17], while we would like to emphasize that the statistic condition does not affect the stability mechanism of the quantum droplet, which is mainly determined by intra-atomic interaction. When the  $p$ -wave interaction strength is far larger than the background-interaction strengths, i.e., the effective  $p$ -wave interaction strength  $g_p = m\bar{g}^2 \gg g_{aa}, g_{am}, g_{mm}$ , we have  $E_0/V = -\frac{(2\epsilon_0 + \bar{g}^2 m)^2}{16\bar{g}^2 m} + O(\delta_{aa}, \delta_{am}, \delta_{mm})$  with  $\delta_{aa,am,mm} = g_{aa,am,mm}/m\bar{g}^2$ , which implies that the mean-field instability should exist in a finite regime of background-interaction parameters.

On the other hand, since the LHY corrections of  $s$ -wave interactions are typically proportional to  $(g_s n)^{2.5}$  with the  $s$ -wave interaction strength  $g_s$  and average density  $n$  [1,13], and that of  $p$ -wave interaction is proportional to  $(g_p n)^{2.5}$  [see Eq. (28)], if the background  $s$ -wave interactions are weak enough with respect to the  $p$ -wave interaction, the background  $s$ -wave interactions should also not qualitatively affect the stabilization of the  $p$ -wave quantum droplet. Therefore, we can believe the presence of weak background  $s$ -wave interactions will not qualitatively affect the main conclusions of this paper. However, we have to point out that, to the best of our knowledge, the complete experimental data for the background interactions in a  $p$ -wave Feshbach resonance (especially the molecule-molecule interactions) are not available currently, and further investigations are necessary for judging if the quantum droplet could emerge under realistic conditions.

## VIII. CONCLUSION

In this paper, we study the quantum fluctuation correction to the ground states of a  $p$ -wave interacting Bose gas. Beginning with the mean-field analysis of the ground states, it is found that the ground states can be divided into three typical phases for different detunings of the molecule channel, i.e., the ASF, AMSF, and MSF phases, where particles are condensed into only the atomic, both the molecular and atomic, and only the molecular channels, respectively. Particularly, we find the ground state is unstable in the AMSF phase. The instability of the ground state in the AMSF phase also manifests itself in the emergence of imaginary long-wavelength Bogoliubov excitation modes. Furthermore, we calculate the LHY correction with the Bogoliubov excitations. We find the LHY correction can stabilize the ground state in the mean-field-unstable regime. That means that the  $p$ -wave interacting Bose gas is self-stabilized at a certain density. Finally, we construct an effective Hamiltonian to characterize the ground state of a finite system. By solving the corresponding GP equation, we find self-stabilized quantum-droplet solutions. Unlike the  $s$ -wave case, the quantum droplet is anisotropic and carries finite momentums because the spatial rotation and the time-reversal symmetries are spontaneously broken. Although only the interspecies  $p$ -wave interaction is considered here, our results could be extended into the case with weak background  $s$ -wave interactions and may be observed in systems like the  $^{85}\text{Rb} - ^{87}\text{Rb}$  Bose mixture [14,15].

## ACKNOWLEDGMENTS

The authors are indebted to Wei Yi, Chao Gao, Jing-Bo Wang, and Fang Qin for helpful discussion. This work is supported by AFOSR Grant No. FA9550-16-1-0006, MURI-ARO Grant No. W911NF17-1-0323, ARO Grant No. W911NF-11-1-0230 (Z.L. and W.V.L.), the National Postdoctoral Program for Innovative Talents of China (Grant No. BX201700156), the National Natural Science Foundation of China (Grants No. 11904228 and No. 11804221) (J.-S.P.), the Science and Technology Commission of Shanghai Municipality (Grant No. 16DZ2260200), the National Natural Science Foundation of China (Grant No. 11655002) (J.-S.P. and W.V.L.), and the Overseas Scholar Collaborative Program of NSF of China through Grant No. 11429402, sponsored by Peking University (W.V.L.). J.-S.P. also acknowledges support by Xiong-Jun Liu's group during his visit to Peking University.

[1] D. S. Petrov, *Phys. Rev. Lett.* **115**, 155302 (2015).  
 [2] G. Semeghini, G. Ferioli, L. Masi, C. Mazzinghi, L. Wolswijk, F. Minardi, M. Modugno, G. Modugno, M. Inguscio, and M. Fattori, *Phys. Rev. Lett.* **120**, 235301 (2018).  
 [3] P. Cheiney, C. R. Cabrera, J. Sanz, B. Naylor, L. Tanzi, and L. Tarruell, *Phys. Rev. Lett.* **120**, 135301 (2018).  
 [4] C. Cabrera, L. Tanzi, J. Sanz, B. Naylor, P. Thomas, P. Cheiney, and L. Tarruell, *Science* **359**, 301 (2018).  
 [5] Y. V. Kartashov, B. A. Malomed, L. Tarruell, and L. Torner, *Phys. Rev. A* **98**, 013612 (2018).

[6] I. Ferrier-Barbut, H. Kadau, M. Schmitt, M. Wenzel, and T. Pfau, *Phys. Rev. Lett.* **116**, 215301 (2016).  
 [7] H. Kadau, M. Schmitt, M. Wenzel, C. Wink, T. Maier, I. Ferrier-Barbut, and T. Pfau, *Nature (London)* **530**, 194 (2016).  
 [8] L. Chomaz, S. Baier, D. Petter, M. J. Mark, F. Wächtler, L. Santos, and F. Ferlaino, *Phys. Rev. X* **6**, 041039 (2016).  
 [9] M. Schmitt, M. Wenzel, F. Böttcher, I. Ferrier-Barbut, and T. Pfau, *Nature (London)* **539**, 259 (2016).  
 [10] A. Bulgac, *Phys. Rev. Lett.* **89**, 050402 (2002).  
 [11] Y. Sekino and Y. Nishida, *Phys. Rev. A* **97**, 011602(R) (2018).

- [12] X. Cui, *Phys. Rev. A* **98**, 023630 (2018).
- [13] K. H. T. D. Lee and C. N. Yang, *Phys. Rev.* **106**, 1135 (1957).
- [14] S. B. Papp, J. M. Pino, and C. E. Wieman, *Phys. Rev. Lett.* **101**, 040402 (2008).
- [15] S. Dong, Y. Cui, C. Shen, Y. Wu, M. K. Tey, L. You, and B. Gao, *Phys. Rev. A* **94**, 062702 (2016).
- [16] L. Radzihovsky and S. Choi, *Phys. Rev. Lett.* **103**, 095302 (2009).
- [17] S. Choi and L. Radzihovsky, *Phys. Rev. A* **84**, 043612 (2011).
- [18] E. Aybar and M. O. Oktel, *Phys. Rev. A* **99**, 013620 (2019).
- [19] N. Bogoliubov, *J. Phys. (USSR)* **11**, 23 (1947).
- [20] C. J. Pethick and H. Smith, *Bose-Einstein Condensation in Dilute Gases*, 2nd ed. (Cambridge University Press, Cambridge, UK, 2008).
- [21] V. Gurarie and L. Radzihovsky, *Ann. Phys.* **322**, 2 (2007).
- [22] F. Qin, *Phys. Rev. A* **98**, 053621 (2018).
- [23] C. Luciuk, S. Trotzky, S. Smale, Z. Yu, S. Zhang, and J. H. Thywissen, *Nat. Phys.* **12**, 599 (2016).